Letter

Zigzag magnetic order in the Kitaev spin-liquid candidate material $RuBr_3$ with a honeycomb lattice

Yoshinori Imai,[1,*] Kazuhiro Nawa,[2] Yasuhiro Shimizu,[3] Wakana Yamada,[1] Hideyuki Fujihara,[1] Takuya Aoyama,[1] Ryotaro Takahashi,[2] Daisuke Okuyama,[2] Takamasa Ohashi,[3] Masato Hagihala,[4] Shuki Torii,[4] Daisuke Morikawa,[2] Masami Terauchi,[2] Takayuki Kawamata,[5] Masatsune Kato,[5] Hirotada Gotou,[6] Masayuki Itoh,[3] Taku J. Sato,[2] and Kenya Ohgushi[1]

[1]*Department of Physics, Graduate School of Science, Tohoku University, 6-3 Aramaki-Aoba, Aoba-ku, Sendai, Miyagi 980-8578, Japan*
[2]*Institute of Multidisciplinary Research for Advanced Materials, Tohoku University, Katahira, Aoba-ku, Sendai, Miyagi 980-8577, Japan*
[3]*Department of Physics, Nagoya University, Furo-cho, Chikusa-ku, Nagoya 464-8602, Japan*
[4]*Institute of Materials Structure Science, High Energy Accelerator Research Organization (KEK), Tokai, Ibaraki 319-1106, Japan*
[5]*Department of Applied Physics, Graduate School of Engineering, Tohoku University, Aoba-ku, Sendai, Miyagi 980-8579, Japan*
[6]*Institute for Solid State Physics, University of Tokyo, Kashiwa, Chiba 277-8581, Japan*

(Received 16 September 2021; revised 27 December 2021; accepted 7 January 2022; published 26 January 2022)

We successfully synthesize $RuBr_3$, which is a candidate material of a Kitaev spin liquid, via a high-pressure synthesis. The material $RuBr_3$ possesses a BiI_3-type structure (space group $R\bar{3}$) where Ru^{3+} forms an ideal honeycomb lattice even at room temperature and it does not show a structural transition at low temperatures. $RuBr_3$ has a negative Weiss temperature and it undergoes a zigzag antiferromagnetic transition at $T_N = 34$ K, as does α-$RuCl_3$ ($T_N = 7$–14 K) which is a promising candidate for a Kitaev spin liquid. Although both compounds of $RuBr_3$ and α-$RuCl_3$ have a zigzag magnetic order at low temperature, the magnetic order in $RuBr_3$ is more robust than in α-$RuCl_3$. Our results indicate that the Kitaev and non-Kitaev interactions can be modified in ruthenium trihalides by changing the ligand sites, and will provide another platform for exploring Kitaev spin liquids.

DOI: 10.1103/PhysRevB.105.L041112

A theoretical breakthrough [1] has brought compounds with honeycomb lattices into the spotlight as candidates for quantum spin liquids. Kitaev proposed a model where $S = 1/2$ spins placed on a honeycomb lattice are coupled with their three nearest-neighbor spins with bond-dependent ferromagnetic Ising interactions [1]. This model is exactly solvable, and the ground state is a quantum spin liquid. The material α-$RuCl_3$ is the most promising candidate for a Kitaev spin liquid and has been actively studied in recent years [2–4]. In α-$RuCl_3$, Ru^{3+} forms a honeycomb lattice in two-dimensional layers through an edge-sharing network of $RuCl_6$ octahedra. The detailed crystal structure of α-$RuCl_3$ is debated [5–8]. Recent studies on high-quality single crystals report that it has an $AlCl_3$-type crystal structure at room temperature with a slightly distorted honeycomb lattice (space group $C2/m$), and that below a structural transition temperature of 150 K, it has a BiI_3-type structure with an ideal honeycomb lattice [space group $R\bar{3}$, Fig. 1(a)] [9–11]. Instead of the expected spin-liquid state owing to the frustrated nature of the Kitaev interaction K, α-$RuCl_3$ shows a zigzag antiferromagnetic order [6]. The antiferromagnetic transition temperature, $T_N = 7$–14 K, is very sensitive to the details of the crystal structure [7,12]. The long-range antiferromagnetic order originates from the sizable contributions of non-Kitaev interactions such as the Heisenberg interaction J and off-diagonal interaction Γ. In fact, the extended model that takes such contributions into account (the J-K-Γ model) is useful for describing the magnetic properties of α-$RuCl_3$. The Hamiltonian is written as

$$\mathcal{H} = \sum_{\langle i,j\rangle \in \mathrm{NN}} \left[J\boldsymbol{S}_i \cdot \boldsymbol{S}_j + K S_i^{\gamma} S_j^{\gamma} + \Gamma\left(S_i^{\alpha} S_j^{\beta} + S_i^{\beta} S_j^{\alpha}\right)\right], \quad (1)$$

where S_i^{γ} denotes the γ component of the spin-1/2 operator of site i (γ being the direction perpendicular to the edge-sharing plane) [13–15]. By assuming appropriate values of the parameters J, K, and Γ, this Hamiltonian [Eq. (1)] can well explain various magnetic behaviors of α-$RuCl_3$, including the zigzag antiferromagnetic order, the field-induced Kitaev spin-liquid state, and magnetic excitations in Raman and inelastic neutron spectra [13,16–18]. Earlier works have revealed a dominant ferromagnetic Kitaev interaction of $K = -3$ to -25 meV and sizable contributions from the other terms, $|J/K| \sim 0.05$–0.25 and $|\Gamma/K| \sim 0.21$–0.99 [19]. Hence, α-$RuCl_3$ is still far from the ideal Kitaev limit, $|K| \gg |J|, |\Gamma|$. However, no methods to tune the parameters J, K, and Γ have been established experimentally, and no state closer to the Kitaev limit has been achieved yet. This is partly because there are no analog materials for α-$RuCl_3$.

Here, we focus on two polymorphs of $RuCl_3$: an α one with a honeycomb structure and a β one with a one-dimensional chain structure (space group $P6_3/mcm$) [20]. While both polymorphs exist for $RuCl_3$, only the chain structure is known for $RuBr_3$ [20,21]. Because α-$RuCl_3$ is more densely packed than β-$RuCl_3$, one expects that $RuBr_3$ with the honeycomb structure can be obtained by keeping $RuBr_3$ with the chain structure under high pressure and high temperature. Actually, recent first-principles calculations predict the stability of

*imai@tohoku.ac.jp

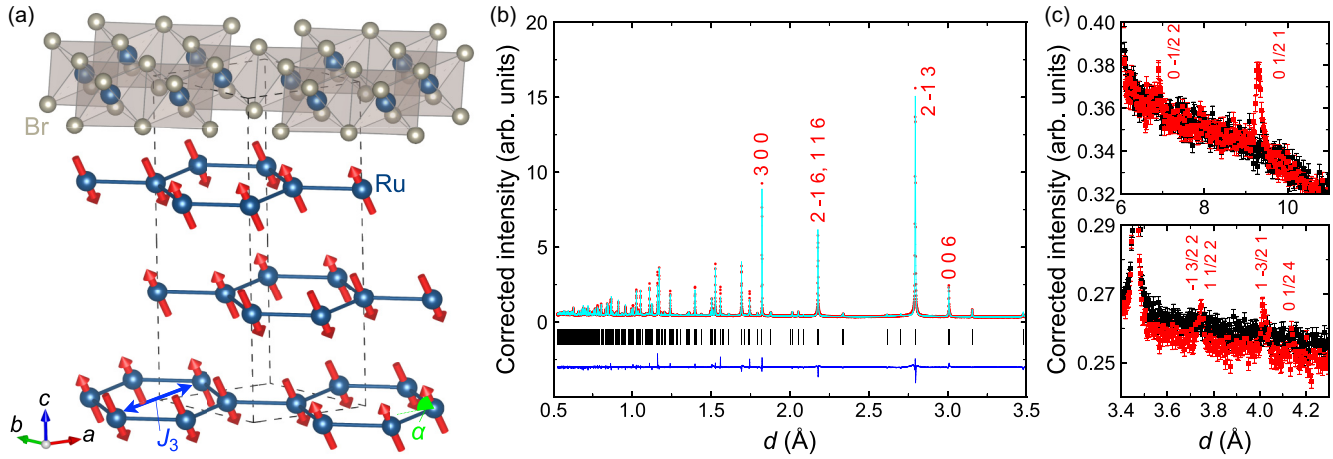

FIG. 1. (a) Schematic of crystal and magnetic structures refined from the neutron diffraction pattern. This figure is drawn using VESTA [53]. α is the angle of the magnetic moment from the honeycomb plane, and J_3 is the third-nearest-neighbor Heisenberg interaction. (b) Neutron diffraction pattern collected at 300 K by the backscattering (BS) bank. The red dots, cyan curve, and blue curve represent the observed intensities, calculated intensities, and difference between them. The difference is shifted for clarity. The vertical black bars indicate the peak position expected from the space group $R\bar{3}$. (c) Neutron diffraction patterns focused on the magnetic reflections. Intensities at 3 and 100 K are represented by the red and black dots, respectively. The upper and lower panels are data collected by the quarter-angle (QA) and low-angle (LA) detector banks, respectively.

$RuBr_3$ with the honeycomb structure, which can be foiled into a monolayer limit [22]. Replacing Cl with Br is expected to have two effects: lattice expansion owing to the larger ionic radius of Br^- than that of Cl^-, and increased covalency of Ru-Cl/Br bonds owing to the up-floating of Br $4p$ bands compared with Cl $3p$ bands. As will be discussed later, both effects bring the system closer to the $|K| \gg |J|, |\Gamma|$ regime.

The $RuBr_3$ polycrystalline sample with a honeycomb lattice was synthesized using a cubic-anvil high-pressure apparatus. The starting material, $RuBr_3$ with the chain structure, was placed in a gold or platinum capsule and loaded into a pyrophyllite cube. These were pressurized at ∼4 GPa and heated at ∼400 °C for 30 min. The electrical resistivity was measured using the four-terminal method. Magnetic susceptibility measurements were performed using a superconducting quantum interference device magnetometer. The specific heat was measured using the thermal-relaxation method. Powder neutron diffraction experiments were performed using the high-resolution time-of-flight (TOF) neutron powder diffractometer SuperHRPD installed at the beamline BL08 of J-PARC [23]. The nuclear quadrupole resonance (NQR) spectra were measured with the spin-echo method with a pulse interval $\tau = 15$–20 μs and $\pi/2$ duration $= 1.5$–2 μs at zero field.

The x-ray diffraction pattern of $RuBr_3$ synthesized at high pressure is totally different from that of $RuBr_3$ with the chain structure. To clarify the crystal structure, we measured the high-resolution neutron powder diffraction at various temperatures; the pattern collected at 300 K is shown in Fig. 1(b). Among several crystal structures with different stacking sequences of the transition-metal trihalides [24–27], the BiI_3 structure with the space group $R\bar{3}$ [Fig. 1(a)] best reproduces the experimental data. We cannot find any signatures of a structural transition such as peak splitting down to 3 K. The crystallographic data obtained through the Rietveld analysis using the FULLPROF software suite [28] are summarized in the Supplemental Material [29] (see also Refs. [30–38] therein). In the refined structure, the Ru atoms in the unit cell are related to each other through the threefold rotation axis along the c direction, and the network formed by the nearest-neighbor Ru-Ru bonds is a regular honeycomb lattice. This indicates that this recently developed $RuBr_3$ provides an ideal platform for exploring Kitaev spin liquids. Henceforth, we discuss the electronic properties of $RuBr_3$ with the $R\bar{3}$ structure.

Figure 2(a) shows the temperature dependence of the resistivity ρ for $RuBr_3$. The data show a thermally activated temperature dependence, which is consistent with a strongly spin-orbital-coupled Mott insulator. The activation energy is $E_g \sim 0.21$ eV. Figure 2(b) shows the temperature dependence of the magnetic susceptibility χ under a magnetic field of $\mu_0 H = 1$ T. The data at 200–300 K well follow Curie-Weiss behavior, $\chi = C_{\rm CW}/(T - \theta_{\rm CW})$, with a Curie constant of $C_{\rm CW} = 0.699$ emu/mol and a Weiss temperature of $\theta_{\rm CW} = -58$ K. The effective moment per ruthenium ion $\mu_{\rm eff}$ is calculated to be $2.36\mu_{\rm B}$ from the relation $C_{\rm CW} = N_{\rm A}\mu_{\rm eff}^2/3k_{\rm B}$, where $N_{\rm A}$ and $k_{\rm B}$ are the Avogadro constant and the Boltzmann constant, respectively. The negative Weiss temperature indicates the predominance of the antiferromagnetic correlation in this system. Turning to the low-temperature regime, χ shows a broad peak around $T^* = 60$ K, which is most likely related to the development of antiferromagnetic correlations. When the system is cooled further, χ shows a kink characterized by a sharp peak in $d\chi/dT$ at $T_{\rm N} = 34$ K, as shown in Fig. 3(a). This kink anomaly corresponds to the formation of long-range antiferromagnetic order. This interpretation is supported by the result for the specific heat C, which shows a peak just around 34 K as shown in Fig. 3(b). The low-temperature part of C obeys a T^3 law ($C = \beta T^3$) as shown in the inset of Fig. 3(b), which can be explained by contributions from Debye phonons and antiferromagnetic spin

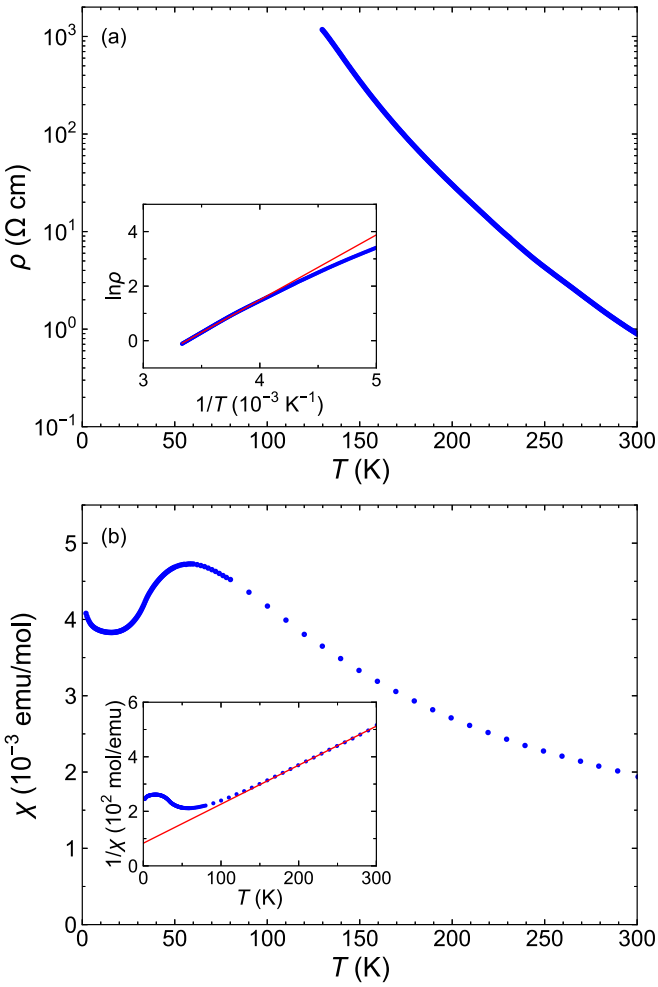

FIG. 2. (a) Temperature (T) dependence of the resistivity (ρ). The inset shows the Arrhenius plot, and the fitting result is shown by the red line. (b) Temperature dependence of the magnetic susceptibility (χ) under a magnetic field of $\mu_0 H = 1$ T. The inset shows the inverse of χ. The data at 200–300 K are fitted with the Curie-Weiss law, and the fitting results are shown by the red line.

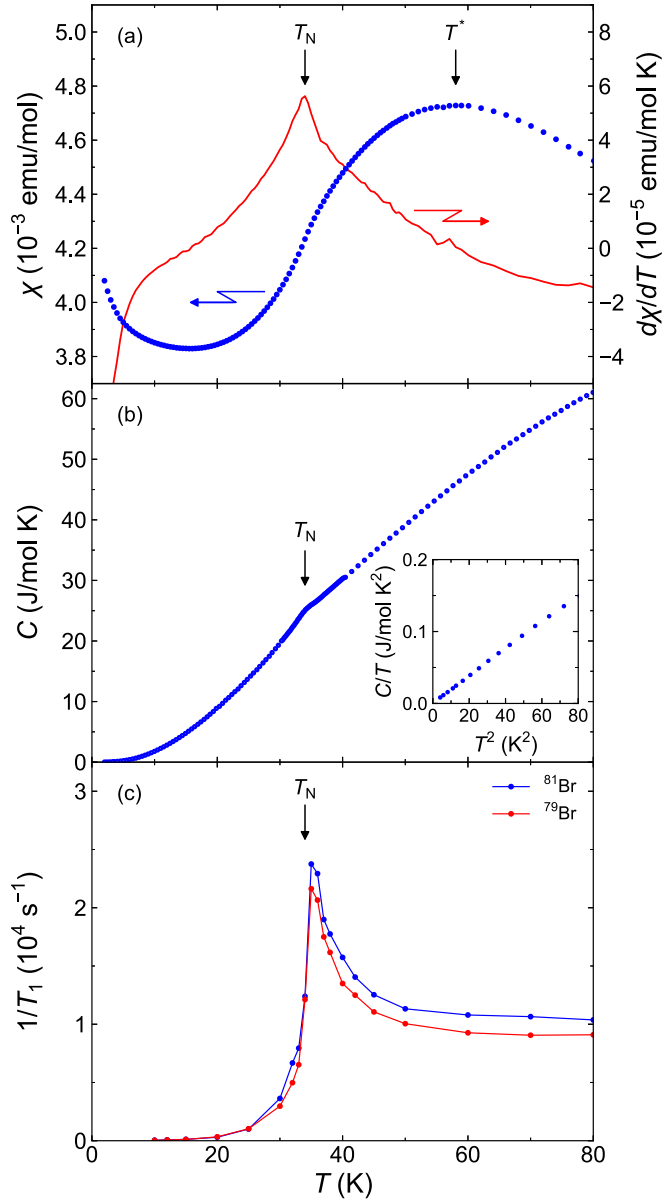

FIG. 3. (a)–(c) Temperature (T) dependences of (a) the magnetic susceptibility (χ) and temperature differential of χ ($d\chi/dT$) under a magnetic field of $\mu_0 H = 1$ T, (b) the specific heat (C) under a zero magnetic field, and (c) the ^{79}Br and ^{81}Br nuclear spin-lattice relaxation rate $1/T_1$. In the inset of (b), C/T is plotted as a function of T^2. The solid curves in (c) are guides for the eye.

waves in three dimensions. If we suppose that spin-wave contributions are negligible, we obtain a Debye temperature of $\theta_D = 159$ K from the formula $\beta = 12\pi^4 NR/5\theta_D^3$, where N is the number of atoms per formula unit and R is the gas constant.

To investigate the spin dynamics, we performed NQR spectroscopy. Figures 4(a) and 4(b) show NQR spectra of ^{81}Br and ^{79}Br (nuclear spin $I = 3/2$) for $RuBr_3$ at 40–280 K. The resonance frequency scales well with the electric quadrupole moment ($^{81}Q = 0.276b$, $^{79}Q = 0.330b$, $b = 10^{-28}$ m^2). A single NQR spectrum for each nucleus is consistent with an $R\bar{3}$ structure that contains one Br site. The temperature dependence of the NQR frequency reflects an enhancement of the electric field gradient via thermal lattice contraction. Upon further cooling, the NQR spectrum splits below 34 K, clearly showing the emergence of a spontaneous local field due to the antiferromagnetic order. Figure 3(c) shows the temperature dependence of the ^{79}Br and ^{81}Br nuclear spin-lattice relaxation rate $1/T_1$. The values for both isotopes scale well with the square of the gyromagnetic ratio, as expected for predominant spin fluctuations. An increase in $1/T_1$ from about 60 K shows the growth of antiferromagnetic correlation; this is in harmony with the broad peak structure at T^* in χ. The spin fluctuations divergently increase toward T_N, below which magnetic excitation is gapped, coinciding with the evolution of the order parameter as observed in the zero-field nuclear magnetic resonance (NMR) spectrum [Fig. 4(c)].

To reveal the magnetic structure, we performed neutron diffraction measurements at low temperature, and the collected patterns are shown in Fig. 1(c). At least five peaks are found at 3 K that do not appear at 100 K. These peaks can be

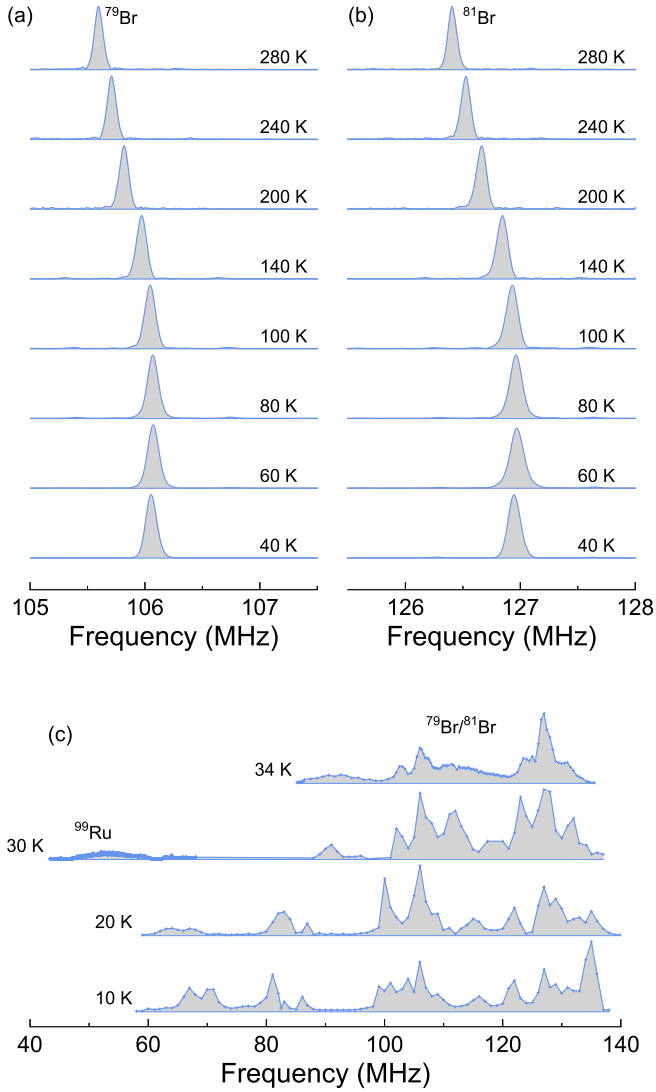

FIG. 4. (a), (b) NQR spectra of (a) ^{79}Br and (b) ^{81}Br above the antiferromagnetic transition temperature. (c) Zero-field Br and Ru nuclear magnetic resonance (NMR) spectra in the antiferromagnetically ordered state. A spectrum below 75 MHz comes from a ^{99}Ru NMR spectrum.

indexed with the magnetic modulation vector $\mathbf{k} = (0, 1/2, 1)$. Initial candidates for determining the magnetic structure were obtained using magnetic representation theory [39]. The magnetic representations for the Ru moments were decomposed into two one-dimensional representations (IR1 and IR2) of the $\mathbf{k}$ group with the magnetic modulation vector $\mathbf{k} = (0, 1/2, 1)$ (see the Supplemental Material [29] for the details of the IRs). The powder neutron diffraction pattern was well fit with the IR2 representation, which represents a zigzag antiferromagnetic structure [Fig. 1(a)]. A zigzag order at low temperature in $RuBr_3$ agrees with the theoretical prediction, which takes electron correlation into account [22]. The magnetic moment is tilted, and its angle from the ab plane is $\alpha = 64(12)^\circ$ [Fig. 1(a)]. The magnitude of the magnetic moment is estimated to be $m = 0.74(12)\mu_B$.

We here compare the experimental results for two honeycomb-based materials, $RuBr_3$ and α-$RuCl_3$. The material $RuBr_3$ has the $R\bar{3}$ structure in the whole temperature range below room temperature, contrasting with the structural transition at 150 K from the $C2/m$ to the $R\bar{3}$ structure in α-$RuCl_3$ [9–11]. The metal-metal bond distance is $d_{\text{Ru-Ru}} = 3.6438(2)$ Å in $RuBr_3$, which is much longer than the reported values $d_{\text{Ru-Ru}} = 3.43$ and 3.46 Å in α-$RuCl_3$ [6,7,40]. The interlayer distance between the honeycomb planes is $d_\perp = 6.014(1)$ Å in $RuBr_3$, which is also longer than the reported $d_\perp = 5.72$ Å in α-$RuCl_3$ [6,7,40]. These are the consequences of the larger ionic radius of Br^- than that of Cl^-. The Ru-Cl/Br-Ru bond angle, which is an indicator of trigonal distortion, is closer to the ideal value of 90° for $RuBr_3$ [$\phi = 93.14(8)^\circ$] than for α-$RuCl_3$ ($\phi \sim 94^\circ$) [6,7]. Hence, the $J_{\text{eff}} = 1/2$ state is still a good starting point in $RuBr_3$, which is also evidenced by the comparable effective magnetic moment: $\mu_{\text{eff}} = 2.36\mu_B$ for $RuBr_3$ and $\mu_{\text{eff}} = 2.24\mu_B$ for α-$RuCl_3$. The crucial difference between the two materials is the dominant magnetic interaction. In $RuBr_3$, there are fairly strong antiferromagnetic interactions characterized by a negative Weiss temperature of $\theta_{\text{CW}} = -58$ K; in α-$RuCl_3$, there are ferromagnetic interactions characterized by a positive Weiss temperature of $\theta_{\text{CW}} = 19$ K. Nevertheless, both compounds have zigzag magnetic order at low temperature. The magnetic order in $RuBr_3$ is more robust than in α-$RuCl_3$. This can be seen from the differences in T_N ($T_N = 34$ K for $RuBr_3$ and $T_N = 7$–14 K for α-$RuCl_3$] and the ordered magnetic moment [$m = 0.74(12)\mu_B$ for $RuBr_3$ and $m = 0.4$–$0.7\mu_B$ for α-$RuCl_3$ [6–8,10]]. The tilt angle of the magnetic moment from the honeycomb plane is $\alpha = 64(12)^\circ$ in $RuBr_3$, which is larger than $\alpha = 32$–35° in α-$RuCl_3$ [7,41]. Concerning magnetic fluctuations above T_N, both materials show an enhancement in $1/T_1$ toward T_N below nearly the same temperature, ~60 K [11]. However, the broad peak structure in the χ curve in this temperature regime is only seen in $RuBr_3$.

We now discuss the microscopic origin of the similarity/difference in magnetic properties of $RuBr_3$ and α-$RuCl_3$. The J-K-Γ model [Eq. (1)] contains the zigzag magnetic order as the ground state in a wide parameter space. Let us first discuss how the replacement of Cl with Br influences J, K, and Γ. The leading terms of J, K, and Γ deduced from perturbation theory can be written as follows [13,42–45],

$$J \simeq \frac{4}{9}\frac{t_{dd}^2}{U}, \quad K \simeq -\frac{8}{3}\frac{t_{dpd}^2}{U}\frac{J_H}{U}, \quad \Gamma \simeq -\frac{16}{9}\frac{t_{dpd}t_{dd}}{U}\frac{J_H}{U}, \quad (2)$$

where U and J_H are the Coulomb repulsion and the Hund's coupling between t_{2g} electrons at the same site, respectively. These exchange interactions are sensitive to the direct hopping between nearest-neighbor t_{2g} orbitals, t_{dd}, and the indirect hopping between nearest-neighbor t_{2g} orbitals via ligand p orbitals, t_{dpd}. Replacing Cl with Br brings about a drastic change, especially in t_{dd} and t_{dpd}. Because $d_{\text{Ru-Ru}}$ for $RuBr_3$ is much longer than that for α-$RuCl_3$, replacing Cl with Br results in a significant decrease in t_{dd}. The t_{dpd} values would be enhanced by replacing Cl with Br, because Br $4p$ orbitals are more strongly hybridized with Ru $4d$ orbitals than Cl $3p$ orbitals. As a result, $RuBr_3$ is expected to have a larger $|K|$ and smaller $|J/K|$ and $|\Gamma/K|$ than α-$RuCl_3$. Therefore, the argument based on the change in the hopping

parameters implies that replacing Cl with Br drives the system closer to a parameter regime for the Kitaev spin liquid. The likely experimental results to support our hypothesis are a magnetic moment angle (α). Theoretical calculations based on the J-K-Γ model indicate that α monotonically increases by approaching the Kitaev spin-liquid limit in the zigzag antiferromagnetic phase [14,46–48]. Thus, our experimental observation of the larger α in $RuBr_3$ than in α-$RuCl_3$ provides an experimental evidence for a smaller value of $|J/K|$ and $|\Gamma/K|$ in $RuBr_3$. It should be noted, however, that the "pseudomoment" direction, which is theoretically discussed in relation to the Kitaev interaction in Ref. [47], is not exactly the same as the moment angle (α) experimentally obtained by neutron scattering and that α is affected by the anisotropy of the g factors.

Here, the question arises as to why the zigzag antiferromagnetic order in $RuBr_3$ is more stable than in α-$RuCl_3$ despite the increased ferromagnetic Kitaev interaction. One possible answer is that the energy scale of the J-K-Γ model becomes much larger in $RuBr_3$ than in α-$RuCl_3$; however, this idea does not account for the difference in sign of the Weiss temperature between $RuBr_3$ and α-$RuCl_3$. The other plausible reason for the stable magnetic order in $RuBr_3$ is obtained by going beyond the J-K-Γ model. The negative Weiss temperature in $RuBr_3$ implies a significant contribution from the antiferromagnetic non-Kitaev interactions. The possible candidate is the third-nearest-neighbor Heisenberg interaction J_3 (>0), which is shown in Fig. 1(a). This exchange interaction is believed to play an important role in the formation of zigzag antiferromagnetic order [13,44,49,50]. The hopping process responsible for J_3 occurs through Ru $4d$–Br $4p$–Br $4p$–Ru $4d$ path [3,51], which is pronounced owing to the enhanced hopping integrals between Ru $4d$–Br $4p$ and Br $4p$–Br $4p$ orbitals. Let us roughly estimate the energy scale of J_3 from θ_{CW}. In the mean-field approximation, the Weiss temperature for a powder-averaged system is [51,52]

$$k_B\theta_{CW} = -\tfrac{3}{4}\left(J + \tfrac{1}{3}K + J_3\right). \quad (3)$$

If we suppose that J is negligible, we can conclude from the negative Weiss temperature that $|3J_3|$ is at least comparable to K. It should be noted that a recent theoretical study reported that the intrinsic Weiss temperature cannot be evaluated by the standard Curie-Weiss law in the Kitaev candidate material. In order to discuss the microscopic interaction parameters in more detail, it is necessary to analyze the data on the anisotropy of χ by using a modified Curie-Weiss law that takes into account the temperature dependence of μ_{eff}.

It is also important to pay attention to a dimensionality when discussing the reason for the stabilization of the zigzag antiferromagnetic order in $RuBr_3$. Despite the fact that the magnetic structures of α-$RuCl_3$ and $RuBr_3$ are three-dimensional ones, the Hamiltonians of J-K-Γ and J-K-Γ-J_3 models assume complete two-dimensionality and do not take into account any interactions between honeycomb layers. It is plausible to consider that the enhancement of coupling between honeycomb layers causes the increase in T_N. Since the electronegativity of Br is smaller than that of Cl, the electronic structure of $RuBr_3$ becomes a more three-dimensional one, which is the origin of the high T_N in $RuBr_3$. In any case, further experiments, especially on single crystals, are required for understanding the magnetic properties of $RuBr_3$, as well as support from theoretical studies.

In conclusion, we successfully synthesized $RuBr_3$ with a BiI_3-type structure (space group $R\bar{3}$), where Ru^{3+} forms an ideal honeycomb lattice. $RuBr_3$ shows a zigzag antiferromagnetic transition at $T_N = 34$ K, which is significantly higher than $T_N = 7$–14 K in α-$RuCl_3$. The increase of T_N in $RuBr_3$ is probably resulting from the third-nearest-neighbor Heisenberg interaction and/or the interlayer coupling due to the three dimensionality. Our results indicate that the Kitaev and non-Kitaev interactions can be modified in ruthenium trihalides by changing the ligand sites, and provide another platform for exploring Kitaev spin liquids.

We would like to thank Y. Yamaji, T. Misawa, J. Nasu, H. Suzuki, and Y. Motome for fruitful discussions, and T. Hiraoka and T. Yajima for their help in the x-ray diffraction measurements. This work was carried out under the Visiting Researcher's Program of the Institute for Solid State Physics, the University of Tokyo. The neutron diffraction experiments at the Materials and Life Science Experimental Facility of the J-PARC were performed under a user program (Proposal No. 2020A0219). This work was financially supported by JSPS KAKENHI under Grants No. JP18H01159, No. JP18K03531, No. JP19H01834, No. JP19H01837, No. JP19H04685, No. JP19H05822, No. JP19H05823, No. JP19H05824, No. JP19K21837, No. JP19K21839, No. JP20H01850, and No. JP20K14395; by the Murata Science Foundation; by the CORE Laboratory Research Program "Dynamic Alliance for Open Innovation Bridging Human, Environment and Materials" of the Network Joint Research Center for Materials and Device; and by JST CREST under Grant No. JP19198318. Mark Kurban from Edanz Group [54] edited a draft of this manuscript.

[1] A. Kitaev, Ann. Phys. **321**, 2 (2006).
[2] G. Jackeli and G. Khaliullin, Phys. Rev. Lett. **102**, 017205 (2009).
[3] S. M. Winter, A. A. Tsirlin, M. Daghofer, J. van den Brink, Y. Singh, P. Gegenwart, and R. Valentí, J. Phys.: Condens. Matter **29**, 493002 (2017).
[4] Y. Motome and J. Nasu, J. Phys. Soc. Jpn. **89**, 012002 (2020).
[5] E. V. Stroganov and K. V. Ovchinnikov, Vestn. Leningr. Univ., Ser. Fiz. i Khim. **12**, 152 (1957).
[6] R. D. Johnson, S. C. Williams, A. A. Haghighirad, J. Singleton, V. Zapf, P. Manuel, I. I. Mazin, Y. Li, H. O. Jeschke, R. Valentí, and R. Coldea, Phys. Rev. B **92**, 235119 (2015).
[7] H. B. Cao, A. Banerjee, J.-Q. Yan, C. A. Bridges, M. D. Lumsden, D. G. Mandrus, D. A. Tennant, B. C. Chakoumakos, and S. E. Nagler, Phys. Rev. B **93**, 134423 (2016).

[8] A. Banerjee, C. A. Bridges, J.-Q. Yan, A. A. Aczel, L. Li, M. B. Stone, G. E. Granroth, M. D. Lumsden, Y. Yiu, J. Knolle, S. Bhattacharjee, D. L. Kovrizhin, R. Moessner, D. A. Tennant, D. G. Mandrus, and S. E. Nagler, Nat. Mater. **15**, 733 (2016).

[9] Y. Kubota, H. Tanaka, T. Ono, Y. Narumi, and K. Kindo, Phys. Rev. B **91**, 094422 (2015).

[10] S. Y. Park, S. H. Do, K. Y. Choi, D. Jang, T. H. Jang, J. Schefer, C. M. Wu, J. S. Gardner, J. M. S. Park, J. H. Park, and S. Ji, arXiv:1609.05690.

[11] Y. Nagai, T. Jinno, J. Yoshitake, J. Nasu, Y. Motome, M. Itoh, and Y. Shimizu, Phys. Rev. B **101**, 020414(R) (2020).

[12] J. A. Sears, M. Songvilay, K. W. Plumb, J. P. Clancy, Y. Qiu, Y. Zhao, D. Parshall, and Y.-J. Kim, Phys. Rev. B **91**, 144420 (2015).

[13] J. G. Rau, E. K.-H. Lee, and H.-Y. Kee, Phys. Rev. Lett. **112**, 077204 (2014).

[14] J. Chaloupka and G. Khaliullin, Phys. Rev. B **92**, 024413 (2015).

[15] L. Janssen, E. C. Andrade, and M. Vojta, Phys. Rev. B **96**, 064430 (2017).

[16] L. J. Sandilands, Y. Tian, K. W. Plumb, Y.-J. Kim, and K. S. Burch, Phys. Rev. Lett. **114**, 147201 (2015).

[17] J. Nasu, J. Knolle, D. L. Kovrizhin, Y. Motome, and R. Moessner, Nat. Phys. **12**, 912 (2016).

[18] Y. Kasahara, T. Ohnishi, Y. Mizukami, O. Tanaka, S. Ma, K. Sugii, N. Kurita, H. Tanaka, J. Nasu, Y. Motome, T. Shibauchi, and Y. Matsuda, Nature (London) **559**, 227 (2018).

[19] P. Laurell and S. Okamoto, npj Quantum Mater. **5**, 2 (2020).

[20] H. Hillebrecht, T. Ludwig, and G. Thiele, Z. Anorg. Allg. Chem. **630**, 2199 (2004).

[21] H. G. von Schnering, K. Brodersen, F. Moers, H. K. Breitbach, and G. Thiele, J. Less-Common Met. **11**, 288 (1966).

[22] F. Ersan, E. Vatansever, S. Sarikurt, Y. Yüksel, Y. Kadioglu, H. D. Ozaydin, O. Ü. Aktürk, Ü. Akinci, and E. Aktürk, J. Magn. Magn. Mater. **476**, 111 (2019).

[23] S. Torii, M. Yonemura, T. Yulius Surya Panca Putra, J. Zhang, P. Miao, T. Muroya, R. Tomiyasu, T. Morishima, S. Sato, H. Sagehashi, Y. Noda, and T. Kamiyama, J. Phys. Soc. Jpn. **80**, SB020 (2011).

[24] U. Müller, *Inorganic Structural Chemistry*, 2nd ed. (Wiley, Hoboken, NJ, 2006).

[25] U. Müller and E. Conradi, Z. Kristallogr. - Cryst. Mater. **176**, 233 (1986).

[26] H. Hillebrecht, P. Schmidt, H. Rotter, G. Thiele, P. Zönnchen, H. Bengel, H.-J. Cantow, S. Magonov, and M.-H. Whangbo, J. Alloys Compd. **246**, 70 (1997).

[27] M. A. McGuire, Crystals **7**, 121 (2017).

[28] J. Rodríguez-Carvajal, Phys. B: Condens. Matter **192**, 55 (1993).

[29] See Supplemental Material at http://link.aps.org/supplemental/10.1103/PhysRevB.105.L041112 for details on the neutron diffraction, results of powder x-ray diffraction, transmission electron microscopy, magnetic susceptibility and specific heat under various magnetic fields for $RuBr_3$, and electronic properties of polycrystalline α-$RuCl_3$ prepared at high pressure.

[30] R. B. Von Dreele, J. D. Jorgensen, and C. G. Windsor, J. Appl. Crystallogr. **15**, 581 (1982).

[31] P. W. Stephens, J. Appl. Crystallogr. **32**, 281 (1999).

[32] S. Merlino, L. Labella, F. Marchetti, and S. Toscani, Chem. Mater. **16**, 3895 (2004).

[33] B. E. Warren, Phys. Rev. **59**, 693 (1941).

[34] J. Rodríguez-Carvajal, BASIREPS program, ftp://ftp.cea.fr/pub/llb/divers/BasIreps.

[35] M. Tanaka and K. Tsuda, J. Electron Microsc. **60**, S245 (2011).

[36] Y. Zhu, A. Morton, and J. Nie, Acta Mater. **58**, 2936 (2010).

[37] E. Abe, A. Ono, T. Itoi, M. Yamasaki, and Y. Kawamura, Philos. Mag. Lett. **91**, 690 (2011).

[38] H. Suzuki, H. Liu, J. Bertinshaw, K. Ueda, H. Kim, S. Laha, D. Weber, Z. Yang, L. Wang, H. Takahashi, K. Fürsich, M. Minola, B. V. Lotsch, B. J. Kim, H. Yavaş, M. Daghofer, J. Chaloupka, G. Khaliullin, H. Gretarsson, and B. Keimer, Nat. Commun. **12**, 4512 (2021).

[39] Y. Izyumov and V. Naish, J. Magn. Magn. Mater. **12**, 239 (1979).

[40] Y. Imai, K. Konno, Y. Hasegawa, T. Aoyama, and K. Ohgushi, Phys. Rev. B **99**, 245141 (2019).

[41] J. A. Sears, L. E. Chern, S. Kim, P. J. Bereciartua, S. Francoual, Y. B. Kim, and Y.-J. Kim, Nat. Phys. **16**, 837 (2020).

[42] H. Matsuura and M. Ogata, J. Phys. Soc. Jpn. **83**, 093701 (2014).

[43] J. Nasu and Y. Motome, Phys. Rev. B **90**, 045102 (2014).

[44] S. M. Winter, Y. Li, H. O. Jeschke, and R. Valentí, Phys. Rev. B **93**, 214431 (2016).

[45] Y. Motome, R. Sano, S. Jang, Y. Sugita, and Y. Kato, J. Phys.: Condens. Matter **32**, 404001 (2020).

[46] H.-S. Kim and H.-Y. Kee, Phys. Rev. B **93**, 155143 (2016).

[47] J. Chaloupka and G. Khaliullin, Phys. Rev. B **94**, 064435 (2016).

[48] J. Rusnačko, D. Gotfryd, and J. Chaloupka, Phys. Rev. B **99**, 064425 (2019).

[49] V. M. Katukuri, S. Nishimoto, V. Yushankhai, A. Stoyanova, H. Kandpal, S. Choi, R. Coldea, I. Rousochatzakis, L. Hozoi, and J. van den Brink, New J. Phys. **16**, 013056 (2014).

[50] Y. Yamaji, Y. Nomura, M. Kurita, R. Arita, and M. Imada, Phys. Rev. Lett. **113**, 107201 (2014).

[51] L. Janssen, S. Koch, and M. Vojta, Phys. Rev. B **101**, 174444 (2020).

[52] Y. Li, S. M. Winter, D. A. S. Kaib, K. Riedl, and R. Valentí, Phys. Rev. B **103**, L220408 (2021).

[53] K. Momma and F. Izumi, J. Appl. Crystallogr. **44**, 1272 (2011).

[54] See, https://jp.edanz.com/.